

In vivo skin reactions from pulsed-type, bipolar, alternating current radiofrequency treatment using invasive noninsulated electrodes

S.B. Cho^{1,2}  | J. Na³ | Z. Zheng^{1,4} | J.M. Lim⁵ | J.-S. Kang² | J.H. Lee⁵ | S.E. Lee⁵

¹Department of Dermatology and Cutaneous Biology Research Center, International St. Mary's Hospital, Catholic Kwandong University College of Medicine, Incheon, Korea

²Kangskin Dermatology Clinic, Seoul, Korea

³Department of Anatomy, Soonchunhyang University College of Medicine, Cheonan, Korea

⁴Department of Dermatology, Yanbian University Hospital, Yanji, China

⁵Department of Dermatology and Cutaneous Biology Research Institute, Yonsei University College of Medicine, Seoul, Korea

Correspondence

Ju Hee Lee, Department of Dermatology and Cutaneous Biology Research Institute, Severance Hospital, Yonsei University College of Medicine, Seoul, Korea.

E-mail: juhee@yuhs.ac

and

Sang Eun Lee, Department of Dermatology and Cutaneous Biology Research Institute, Gangnam Severance Hospital, Seoul, Korea.

E-mail: jennifer823@yuhs.ac

Abstract

Background: Bipolar, alternating current radiofrequency (RF) conduction using invasive noninsulated electrodes consecutively generates independent tissue coagulation around each electrode and then, the converged coagulation columns.

Methods: Two pulsed-type RF models at the on-time pulse width/pulse pack of 30 and 40 milliseconds were designed to amplify the early stage of RF-induced tissue reaction using hairless mouse skin *in vivo*. Then, structural and ultrastructural changes were evaluated in hairless mouse skin samples at baseline and immediately 1 day, 3 days, 7 days, and 14 days after treatment.

Results: Immediately after pulsed-RF treatment, a few chrysanthemum-like zones of electrothermal coagulation and hypereosinophilic collagen fibers were found in the dermis and dermo-subcutaneous fat junction. Histochemical staining for periodic acid-Schiff and immunohistochemical staining for type IV collagen revealed marked thickening of basement membranes. Transmission electron microscopy demonstrated that pulsed-RF treatment resulted in higher electron-dense and remarkably thicker lamina densa, as well as increases in anchoring fibrils, compared with untreated control specimens. Furthermore, CD31-positive blood vessels were smaller in size with a slit-like luminal appearance, without excessive damage to endothelial cells.

Conclusion: Our data indicated that pulse-type, bipolar RF energy induces structural and ultrastructural changes in basement membranes and vascular components in hairless mouse skin.

KEYWORDS

alternating current, basement membrane, bipolar, blood vessel, invasive, microneedle, pulsed-type radiofrequency

1 | INTRODUCTION

Radiofrequency (RF) devices emitting a high-frequency alternating electrical current induce selective electrothermal reactions in targeted tissues.¹⁻³ Patterns of RF-induced tissue reactions have been shown to vary according to the resistance or impedance of the targeted tissue,

the frequency of the electrical current, monopolar and bipolar modes of RF delivery, and the characteristics of electrodes.^{1,3-6} Additionally, clinicians have found that continuous- and pulsed-type RF treatments elicit different RF-induced tissue reactions.⁷⁻¹⁰

Continuous-type RF irradiation systems have been used for decades. These systems continuously deliver RF energy over a set conduction time to induce selective electro-thermolytic tissue reactions.^{3,7} Continuous RF delivery generates 3 distinctive zones of hyperthermic

Sung Bin Cho and Jongju Na contributed equally to this work.

tissue injury, including a central zone of coagulative necrosis, a peripheral or transitional zone of reversible thermal injury, and normal surrounding tissue.⁷ In the central zone of coagulative necrosis, a high current density around invasive penetrating electrodes raises tissue temperatures between 60°C and 100°C, causing lethal and irreversible thermal tissue injury.⁷ Meanwhile, tissue in the peripheral zone, which surrounds the central zone, reaches temperatures between 41°C and 45°C; the RF-induced electrothermal reactions in this zone are sublethal, but still vulnerable to further injury.⁷ The peripheral zone additionally shows increased blood flow that facilitates the infiltration of inflammatory cells and induces an immune response.^{11,12}

Electromagnetic initiation and propagation of continuous-type, bipolar, alternating current RF-induced tissue reactions have been investigated *in vivo* in micropig skin and *ex vivo* in bovine liver specimens using invasive noninsulated electrodes.⁶ Therein, independent, cocoon-shaped areas of electrothermal coagulation, called a “Na effect,” were characteristically found around each electrode (areas of high current density) upon continuous delivery of RF signals over the conduction times of 120 milliseconds, 200 milliseconds, 300 milliseconds, and 1 second.⁶ At a conduction time of more than 2 seconds, convergent areas of coagulation appeared throughout inter-electrode areas with lower current density.⁶ Furthermore, *in vivo* in micropig skin and *ex vivo* in bovine liver specimens exhibited the characteristic histologic changes of vascular components along the regions directly between the electrodes without distinguishable tissue coagulation.⁶

In this *in vivo* study, we aimed to investigate RF-induced skin reactions, particularly in vascular components and the basement membrane, at shorter or very closed conduction times that would minimize electrothermal reactions around each penetrating electrode. However, we supposed that a single continuous-type pulse of a very short conduction time would not deliver enough RF signal to induce structural and ultrastructural electrothermal changes in *in vivo* micropig skin or *ex vivo* bovine liver tissue. Therefore, pulsed-type RF models were used to amplify the early stage of RF-induced tissue reaction, and the time-course effects of RF treatment were investigated using experimental hairless mouse skin, which has properly sufficient vascular components. To do so, electrical fields of 2 MHz were generated by 2 different settings of pulsed bipolar RF devices: 3 pulse cycles at a gated on-time pulse width of 40 milliseconds and 5 pulse cycles at an on-time pulse width of 30 milliseconds, equipped with invasive noninsulated microelectrodes. Then, structural and ultrastructural changes were evaluated in hairless mouse skin samples at baseline and immediately 1 day, 3 days, 7 days, and 14 days after treatment.

2 | METHODS

2.1 | Pulsed-type, bipolar, alternating current RF using noninsulated microneedle electrodes

A pulsed-type, bipolar, alternating current RF device equipped with noninsulated microneedle electrodes (SYLFIRM; Viol, Kyunggi, Korea) emitting 2-MHz RF oscillations was utilized to evaluate RF tissue reactions on *in vivo* hairless mouse skin. Two pulsed-type bipolar RF

devices were utilized: one emitting 3 pulse cycles at a gated on-time pulse width of 40 milliseconds and a power of 3.3 watts/pulse pack (type A) and the other emitting 5 pulse cycles at an on-time pulse width of 30 milliseconds and a power of 3 watts/pulse pack (type B). Both devices utilized 10 mm × 10 mm disposable tips composed of 25 invasive noninsulated microneedle electrodes uniformly arranged in a 5 × 5 pattern. The microneedles are constructed of surgical stainless steel with 24K gold plating for homogeneous RF conduction and comprise a body diameter of 300 ± 10 μm and a pointed microneedle tip length of 750 ± 10 μm.

2.2 | *In vivo* treatment of hairless mouse skin with invasive pulsed-type, bipolar, alternating current RF

All experimental protocols were approved by the ethics committee of the Yonsei University Institutional Animal Care and Use Committee (2015-0172), and the methods were carried out in accordance with the approved guidelines. Thirty-six, female, specific pathogen-free, hairless mice (SKH-1, Orient Bio Inc., Gyeonggi-do, Korea; 6–8 weeks old) were used in this study. General anesthesia was administered via an intraperitoneal bolus injection of tiletamine/zolazepam (5 mg/kg) and xylazine (2 mg/kg). The backs of the experimental mice were cleansed with a mild soap and 70% alcohol. Then, pulsed-type, bipolar, alternating current RF treatment was performed on the experimental mice at the electrode penetration depth of 3.0 mm over one pass without overlapping. Neither pretreatment topical anesthesia nor posttreatment cooling was applied. The experimental mice were killed for sampling the treated skin in a humane manner according to standard protocols.

2.3 | Histological and immunohistochemical examinations

At baseline and at immediately 1, 3, 7, and 14 days after treatment, skin specimens of full thickness from the hairless mice were obtained for histologic evaluation. Each sample was fixed in 10% buffered formalin and then embedded in paraffin. Hairless mouse skin blocks were cut along the longitudinal plane to detect the insertion axes of the microneedle electrodes and RF-skin tissue interactions. For each treatment setting, 20–30 serial skin tissue sections of 4-μm thickness were prepared and stained with hematoxylin and eosin and periodic acid-Schiff (PAS). Additionally, tissue sections from experimental mice were subjected to immunohistochemical examination for type IV collagen, CD31, and vascular endothelial growth factor (VEGF). The rabbit anti-type IV collagen polyclonal antibody (Abcam, Cambridge, UK) at a dilution of 1:200, the rabbit anti-CD31 polyclonal antibody (Abcam) at a dilution of 1:200, and the rabbit anti-VEGF monoclonal antibody (Abcam) at a dilution of 1:250 were used as primary antibodies. After washing with PBS, the sections were incubated in HRP-conjugated secondary anti-sera at a dilution of 1:100 for 30 minutes. Sections were then lightly counterstained with hematoxylin. Negative controls were obtained by omitting the primary antibody.

2.4 | Western blotting and real-time polymerase chain reaction

Full-thickness skin samples from the mice were homogenized in lysis buffer, and a total of 50 μ g of protein per sample was analyzed by denaturing 10% sodium dodecyl sulfate (SDS)-polyacrylamide gel electrophoresis. Prepared samples were immunoblotted with anti-VEGF antibody (Abcam). Signals were revealed using enhanced chemiluminescence. Additionally, tissue samples were homogenized in TRIzol reagent (Invitrogen Life Technologies, Carlsbad, CA, USA), and total cellular RNA was extracted from tissue samples. RNA was reverse transcribed, and the resulting cDNA was synthesized from 500 ng total RNA using TaKaRa RNA PCR Kit Ver.2.1 (TaKaRa BIO INC., Shiga, Japan). Total RNA was reversely transcribed with the TaqMan Reverse Transcription Reagents (Applied Biosystems, Foster City, CA, USA) according to the manufacturer's protocol. Relative mRNA levels were quantified with the fluorescent TaqMan technology. Polymerase chain reaction (PCR) primer and probe specific for murine VEGF-A (assay ID; Mm00437306_m1) were obtained as TaqMan Gene Expression Arrays (Applied Biosystems). Glyceraldehyde 3-phosphate dehydrogenase and β -actin were used as endogenous controls to normalize the amount of sample RNA. The real-time PCR was performed with equal amounts of cDNA in the GeneAmp 7700 sequence detection system (Applied Biosystems) using the TaqMan Universal PCT Master Mix (Applied Biosystems). Reactions were incubated at 50°C for 2 minutes, at 95°C for 10 minutes followed by 40 cycles of 15 seconds at 95°C and 1 minute at 60°C. Water controls were included to ensure specificity. Each experiment was performed triplicate.

2.5 | Transmission electron microscopy

For transmission electron microscopy (TEM), the specimens were fixed in 50 mM sodium cacodylate buffer (pH 7.4) that contained 2% glutaraldehyde in paraformaldehyde for 30 minutes at 32°C, post-fixed in 1% osmium tetroxide for 2 hours at 4°C, and dehydrated by treatment with a graded series of ethanol. Then, the isolated biopsy specimens were treated with propylene oxide, embedded in Epon according to standard procedures, and localized in semi-thin sections. Sections were cut using Ultracut R Ultratome (Leica, Wetzlar, Germany) and were counterstained with 8% uranyl acetate and lead citrate. TEM was also performed using a JEOL JSM 1011 microscope (Tokyo, Japan) operating at 80 kV. Eight to ten pictures of each specimen were taken.

3 | RESULTS

3.1 | In vivo tissue reactions after invasive, pulsed-type, bipolar RF treatment of hairless mouse skin

First, we evaluated histologic changes in hairless mouse skin over the duration of 14 days after invasive, pulsed-type, bipolar RF treatment (Figure 1). Immediately after the treatment, a few chrysanthemum-like zones of electrothermal coagulation were found in the dermis of skin specimens from mice treated with 3 pulse cycles at a gated on-time pulse width of 40 milliseconds and a power of 3.3 watts/pulse pack (type A-RF treatment group). Collagen bundles within the coagulation zones were basophilic and feathery, and each coagulation zone could be morphologically subdivided into approximately 3 distinguished zones of differing degrees of tissue coagulation. No

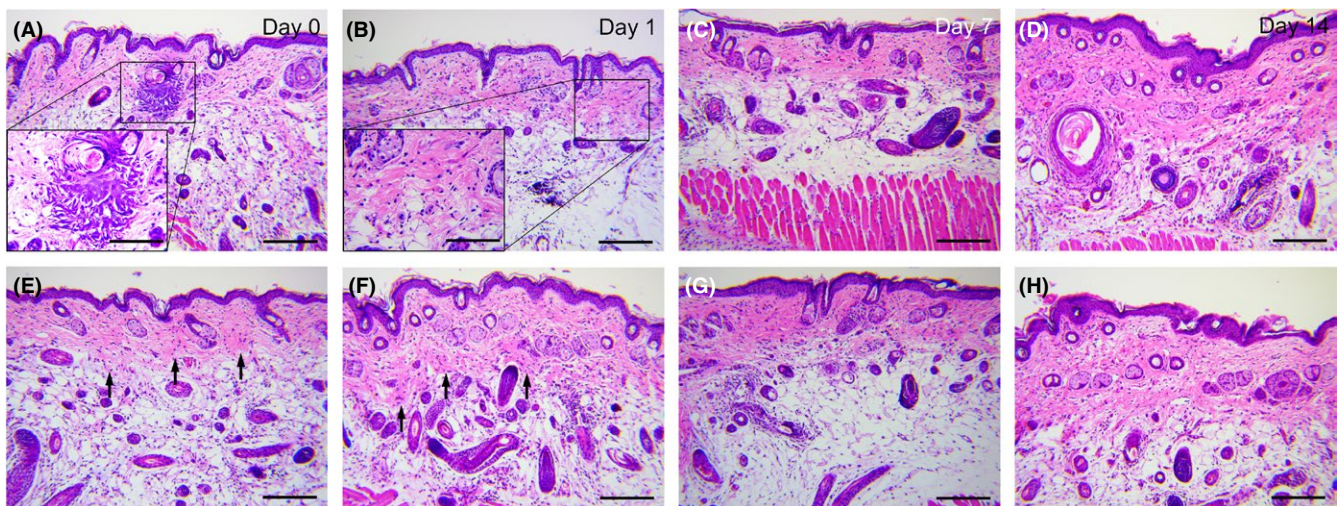


FIGURE 1 *In vivo* tissue reactions from invasive, pulsed-type, bipolar RF in hairless mouse skin. (A-D) Pulsed radiofrequency (RF) treatment with 3 pulse cycles at a gated on-time pulse width of 40 milliseconds and a power of 3.3 watts/pulse pack (Type A). (E-H) Pulsed RF treatment with 5 pulse cycles at an on-time pulse width of 30 milliseconds and a power of 3 watts/pulse pack (Type B). (A) Insets show magnified areas of chrysanthemum-like zones of electrothermal coagulation on day 0 and (B) hypereosinophilic collagen fibers with cellular infiltration on day 1. (E, F) Type B-pulsed RF induced distinguishable hypereosinophilic collagen fibers in the deep dermis and around the dermo-subcutaneous fat junction (arrows). Post-RF (A, E) day 0, (B, F) day 1, (C, G) day 7, and (D, H) day 14. Hematoxylin and eosin stain, original magnification $\times 100$, scale bar = 200 μ m; inset, scale bar = 100 μ m

remarkable focal zones of coagulation necrosis were observed along the epidermis and dermis throughout serially sectioned specimens of mouse skin treated with 5 pulse cycles at an on-time pulse width of 30 milliseconds and a power of 3 watts/pulse pack (type B-RF treatment group). Distinguishable hypereosinophilic collagen fibers, however, were found in the deep dermis and around the dermo-subcutaneous fat junction in both treatment settings, compared to skin at baseline. Furthermore, the thicknesses of the epidermis and dermis increased, and dermal collagen density also notably increased on days 3, 7, and 14.

3.2 | Effects of invasive, pulsed-type, bipolar RF on basement membranes

To investigate structural changes in the basement membrane following pulsed-type, bipolar RF treatment in mouse skin, the expression of type IV collagen and PAS was evaluated. Immunohistochemical staining for type IV collagen highlighted moderate thickening of the basement membrane, which was evident from 3 days after both type A- and type B-RF treatment, compared with untreated control skin (data not shown). By days 7 and 14, marked expression of type IV collagen in the basement membrane was found in both type A- and type B-RF treatment groups, although the expression thereof was more remarkable with type B-RF treatment. Histochemical staining for PAS also revealed moderate increases in the thickness of PAS-positive areas along the BM at posttreatment day 3, compared with untreated control skin, in both type A- and type B-RF treatment groups (Figure 2). Furthermore, PAS-positive thickening of basement membranes was greater at posttreatment days 7 and 14 in both type A- and type B-RF treatment groups, although it was more prominent in skin treated with type B-RF treatment.

3.3 | Transmission electron microscopic features of the basement membrane

Using TEM, we further evaluated structures of the dermo-epidermal junction, including the plasma membranes of basal keratinocytes, lamina lucida, lamina densa, and sublamina densa fibrous components in hairless mouse skin treated with each of the invasive, pulsed-type, bipolar RF devices. In untreated control skin, the lamina densa appeared as a thin and electron-dense rim in the basement membrane (Figure 3). After treatment with the type A- and type B-RF devices, the thickness of the lamina densa increased remarkably beginning on day 3. TEM at posttreatment days 7 and 14 exhibited higher electron-dense and remarkably thicker lamina densa in both type A- and type B-RF-treated skin specimens, compared with untreated control skin. Increases in anchoring fibrils were noted on day 14 in hairless mouse skin treated with type B-RF treatment. Comparing the 2 invasive, pulsed-type, bipolar RF devices, we found that type B irradiation induced more remarkable increases in the thickness of the lamina densa, especially on days 7 and 14.

3.4 | Effects of invasive, pulsed-type, bipolar RF on vascular components

Immunohistochemical stain for the panvascular marker CD31 revealed normal distention of CD31-positive blood vessels with a smooth luminal surface in control mice skin. Meanwhile, immediately and 1 day after RF treatment in both the type A- and type B-RF treatment groups, the CD31-positive blood vessels shrank in size and exhibited luminal structures with a slit-like appearance in the subcutaneous fat layer, but not in the dermis, compared with untreated control skin (Figure 4). The small, collapsed, slit-like CD31-positive blood vessels were noted throughout the dermis and subcutaneous fat layer on days 3 and 7 in both the type A- and type B-RF treatment groups. At 7 days after type B-RF treatment, collapsed vessels were still observed in the upper dermis, while in the deep dermis, vessels appeared to be congested and distended. These vascular component features in the dermis and subcutaneous fat layer were more remarkable on day 14, compared with day 7, particularly with type B-RF treatment. Nonetheless, no signs of excessive damage to vascular components were found for either RF device, and the density of CD31-positive dermal vessels over time was comparable between control mice and RF-treated mice.

3.5 | Effects of invasive, pulsed-type, bipolar RF on vascular endothelial growth factor expression

To examine whether the post-RF treatment alterations in the dermal vascular components were associated with altered expression of VEGF, we assessed VEGF expression in the hairless mouse skin by real-time PCR and western blot analysis. Down-regulation of VEGF-A mRNA expression was found in both type A- and type B-RF treatment groups at posttreatment day 14, compared with untreated control skin, although the difference lacked statistical significance (Figure 5a). Western blot analyses, however, revealed transient over-expression of VEGF protein immediately after treatment that was gradually suppressed over the following 14 days in the type A-RF treatment group, compared with untreated control skin. In the type B-RF treatment group, over-expression of VEGF protein remained throughout the 14 days after treatment, compared with untreated control skin (Figure 5b). Further investigations of VEGF-A expression revealed comparable levels of VEGF-A protein in control and type A-RF treatment skin. In the type B-RF treatment group, VEGF expression in epidermal keratinocytes and dermal vascular components was comparable between untreated control and treated skin, whereas VEGF immunoreactivity was markedly stronger in dermal fibroblasts, compared with control skin (Figure 5c).

4 | DISCUSSION

Pulsed-type RF systems generate thermal and/or nonthermal tissue reactions according to pulse rates and pulse periods between pulse packs.⁸⁻¹⁰ Pulsed-type RF devices can deliver high RF

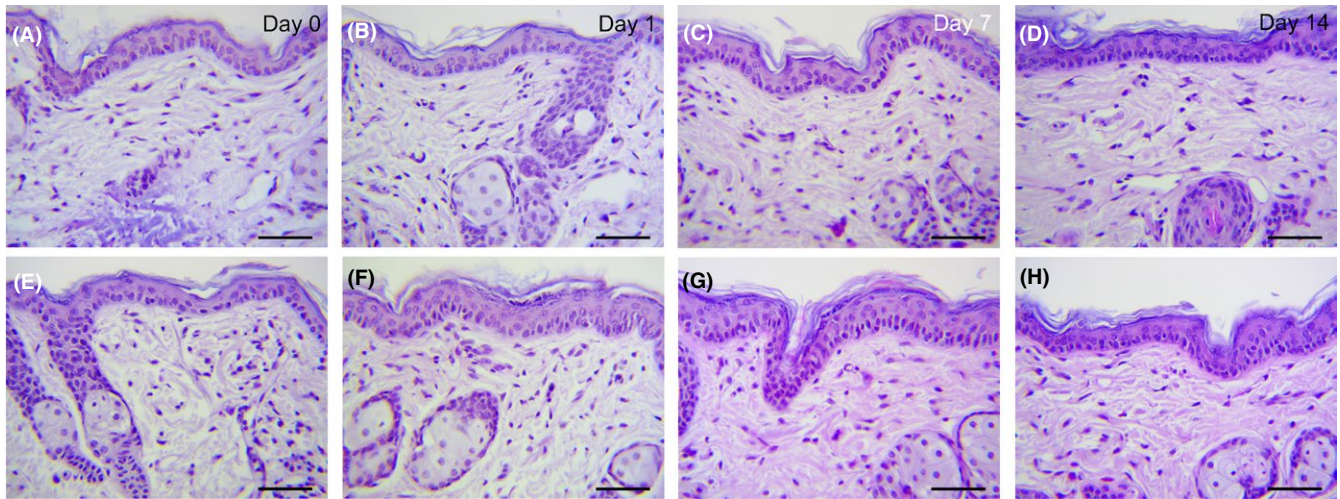


FIGURE 2 Effects of invasive, pulsed-type, bipolar RF on basement membranes. (A-D) Type A-RF treatment group, (E-H) type B-RF treatment group. (C, D, G, H) Skin specimens present increased thickness of periodic acid-Schiff (PAS)-positive areas along the basement membrane (BM) on posttreatment days 7 and 14, which is more remarkable in the type B-RF treatment group. Post-RF (A, E) day 0, (B, F) day 1, (C, G) day 7, and (D, H) day 14. PAS stain, original magnification $\times 400$, scale bar = 50 μm

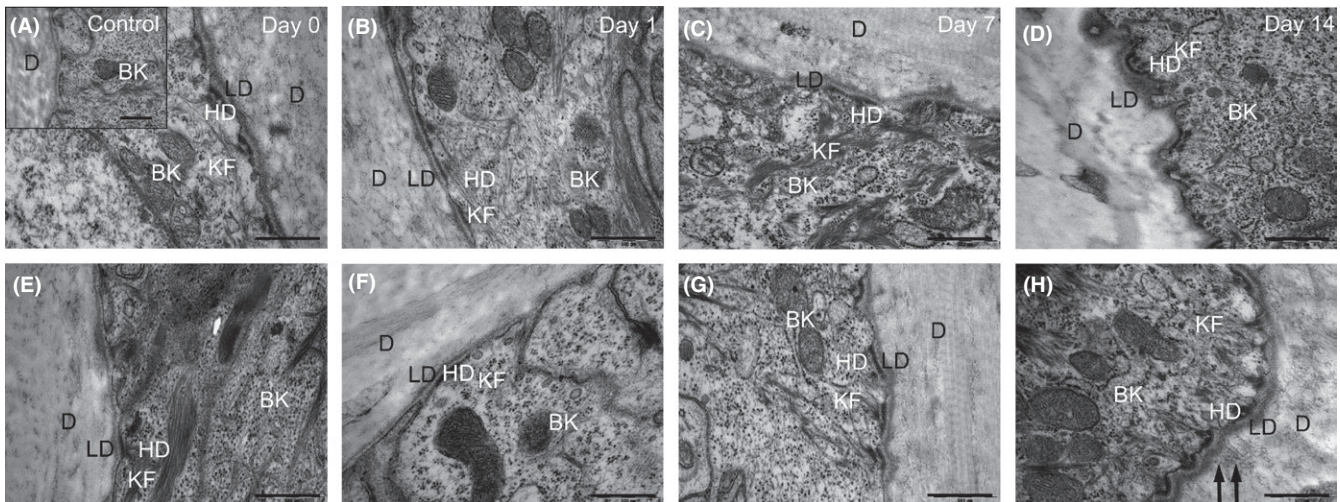


FIGURE 3 Transmission electron microscopic features of basement membranes. (A-D) Type A-RF treatment group, (E-H) type B-RF treatment group. (C, D, G, H) Transmission electron microscopy (TEM) photographs present remarkable thickening of lamina densa on posttreatment days 7 and 14, which is more remarkable in the type B-RF treatment group. (A) Inset comprises a TEM photograph of untreated control mouse skin. (H) Prominent increases in anchoring fibrils (arrows) in hairless mouse skin on day 14 after type B-RF treatment. BK, basal keratinocyte; D, dermis; HD, hemidesmosome; KF, keratin filament; LD, lamina densa. Post-RF (A, E) day 0, (B, F) day 1, (C, G) day 7, and (D, H) day 14. Scale bar = 500 nm

voltages in targeted tissues through gated delivery of RF oscillations that minimizes nonselective electrothermal reactions arising from lethal temperatures.^{3,13} Pulsed-type RF energy of a high signal amplitude stimulates the flow of ions, eliciting changes in cellular and subcellular structures. Furthermore, pulsed electric fields have been found to induce electroporation by modulating cell membrane permeability for use in electro-chemotherapy and gene transfer.⁸⁻¹⁰ However, the effects of invasive, pulsed-type, bipolar, alternating current RF energy on the skin, which is a multi-layered, adnexa-rich, heterogeneous tissue, have not been fully elucidated.

In this study, RF-induced reactions in *in vivo* hairless mouse skin were investigated at shorter or very closed conduction times that would minimize the appearance of Na effect around each penetrating electrode using the pulsed-type RF device with the same setting of 2-MHz RF oscillations as in our previous study.⁶ Furthermore, because our study group previously revealed Na effect upon continuous delivery of RF signals over the minimal conduction time of 120 milliseconds, we designed pulsed-type RF device with the pulse width of single pulse pack much shorter than 120 milliseconds (30 and 40 milliseconds), but total on-time pulse width 120 and 150 milliseconds to fit the study purpose. Thereby, 2 different

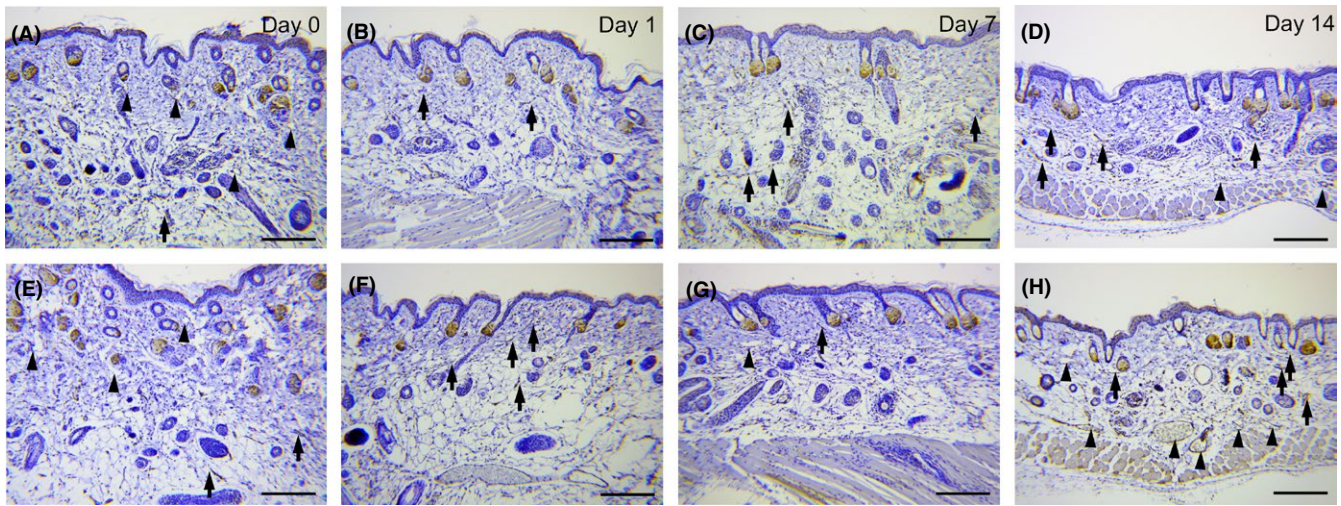


FIGURE 4 Effects of invasive, pulsed-type, bipolar RF on vascular components. (A-D) Type A-RF treatment group, (E-H) type B-RF treatment group. (A, B, E, F) Vascular components small in size and with a slit-like luminal structure (arrows) in the subcutaneous fat layer and distended blood vessels with a smooth luminal surface (arrowheads) in the dermis on days 0 and 1. (C, G) Small and collapsed vascular components throughout the dermis and subcutaneous fat layer on day 7. (D, H) Small and collapsed blood vessels in the dermis and distended blood vessels in the dermis on day 14. Post-RF (A, E) day 0, (B, F) day 1, (C, G) day 7, and (D, H) day 14. CD31-immunohistochemical stain, original magnification $\times 100$, scale bar = 200 μm

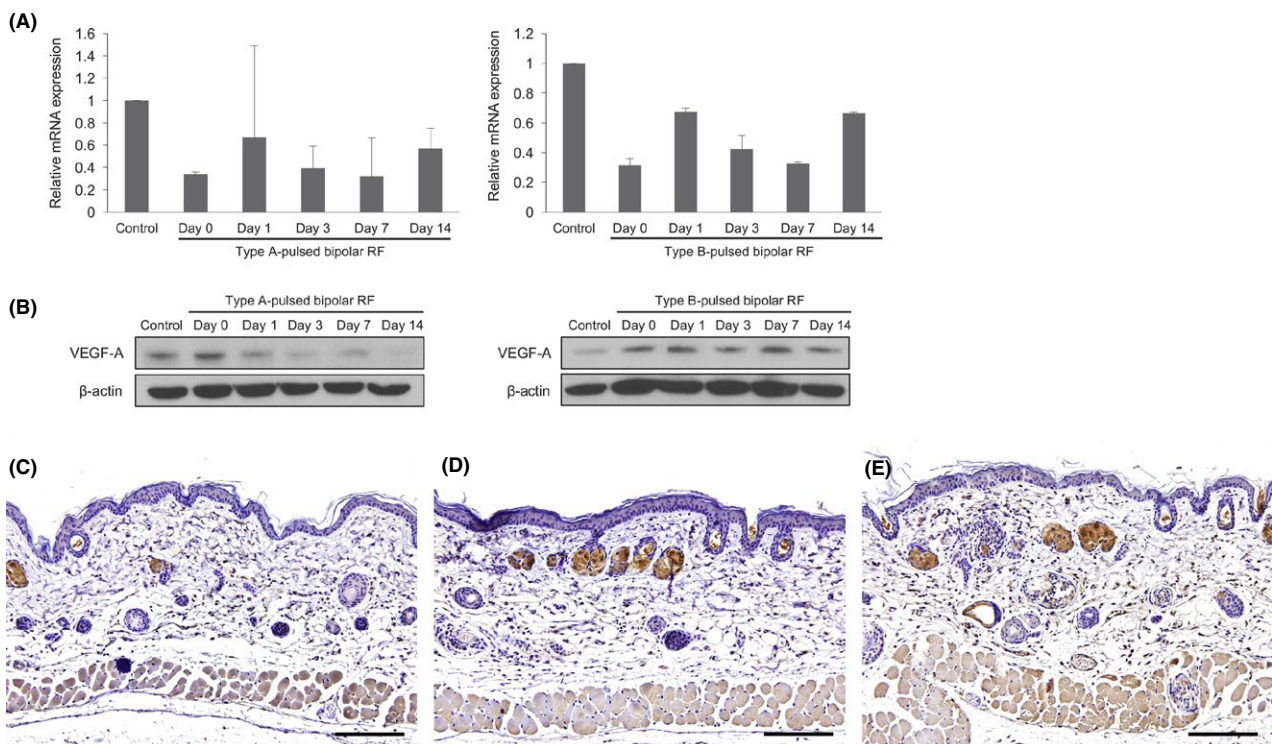


FIGURE 5 Effects of invasive, pulsed-type, bipolar RF on vascular endothelial growth factor expression. (A) Real-time polymerase chain reaction analysis indicates the down-regulation of vascular endothelial growth factor (VEGF)-A mRNA expression in both type A- and type B-RF treatment groups at posttreatment day 14. (B) Western blot analysis reveals tissue expression of VEGF-A in type A- and type B-RF treatment groups. (C-E) VEGF expression in epidermal and dermal components. (C) Untreated control, (D) type A-RF treatment on day 14, and (E) type B-RF treatment on day 14. VEGF-immunohistochemical stain, original magnification $\times 100$, scale bar = 200 μm

settings of pulsed-type, bipolar RF devices were utilized: one to emit 3 pulse cycles at a gated on-time pulse width of 40 milliseconds, 80 000 RF oscillations/pulse pack, and a power of 3.3 watts/pulse

pack and the other to emit 5 pulse cycles at an on-time pulse width of 30 milliseconds, 60 000 RF oscillations/pulse pack, and a power of 3 watts/pulse pack.

The skin shows electrical properties consistent with those of semiconductors.¹⁴ As a multi-layered tissue with a number of different appendage structures, the skin exhibits various current densities that significantly affect tissue impedance and permittivity. Thus, theoretically, conductive RF energy can be utilized to selectively treat vascular components of differing electrical current density.³ Previously, our study group found that bipolar RF-induced tissue reactions are propagated preferentially along the outer layers of dermal vascular components and perivascular structures, which normally exhibit high current density, between electrodes in continuous-type RF treatment.⁶ Thus, in this study, we intended to focus on structural and ultrastructural changes in vascular components and basement membranes induced by pulsed-type RF treatment. Herein, pulsed-type bipolar RF elicited vascular collapse without damaging endothelial cells or causing remarkable electrothermal coagulation in the dermis. The pulsed-type RF-induced selective activation of electrical currents on and around vascular components persisted longer in the upper dermis than in the deep dermis and subcutaneous fat layer. This led us to suggest that pulsed-type delivery of invasive, bipolar, alternating current RF exerts more selective, subcellular, electromagnetic, thermo-modulating effects on the basement membrane and vascular components, compared to those achieved through selective electromagnetic thermolysis by continuous-type bipolar RF.

In the present study, dermal tissue coagulation in the shape of a chrysanthemum was observed only with the 3-pulse RF device. Each coagulation zone could be morphologically subdivided into approximately 3 distinguishable zones of differing degrees of tissue coagulation. In previous studies on continuous RF treatment, we typically observed cocoon-shaped zones of electrothermal coagulation of a relatively homogeneous nature using both insulated and noninsulated penetrating electrodes.^{5,6} However, unlike our previous studies, which were conducted using in vivo micropig skin and ex vivo bovine liver tissue, the present study was conducted using in vivo hairless mouse skin. This may account for the difference in the patterns of dermal tissue coagulation observed in this study.

Electric fields are endogenously generated during wound healing after disruption of the epithelial layer.^{15,16} These electrical fields determine the direction and speed of epithelial cell migration and induce electrotactic responses to dermal fibroblasts and inflammatory cells in a voltage- and time-dependent manner through phosphatase and tensin homolog and phosphatidylinositol-3-OH kinase- γ .¹⁵ Additionally, noninvasive, pulsed electric fields have also been shown to stimulate the secretion of multiple growth factors, thereby leading to the proliferation of epidermal cells, as well as new collagen and vessel formation.¹⁷ In the present study, we found that the electric fields generated by invasive, pulsed-type, bipolar alternating current also increased the thicknesses of the epidermis and dermis with new collagen formation. We suggest that the induction of endogenous electric fields after disruption of the epithelial layer upon penetration of the microneedles and the delivery of exogenous electrical fields may have contributed to these microscopic changes.

5 | CONCLUSION

Our observational study outlined structural and ultrastructural changes in in vivo hairless mouse skin upon delivery of pulsed-type, bipolar, alternating current RF signal via noninsulated microneedle electrodes. The pulsed-type delivery of RF signal at a very short conduction time induced a resistive electrothermal response, starting from the margins of dermal components, such as the basement membrane and blood vessels, just prior to the occurrence of the Na effect around each electrode. However, whether pulsed-type, bipolar, alternating current RF can induce irreversible destruction of targeted vascular components, however, remains to be elucidated. Although the characteristics of hairless mouse skin do not exactly coincide with those of human skin, our findings suggest that pulsed-type RF devices can be used to investigate invasive, bipolar, RF-induced skin reactions elicited over various RF conduction times.

ACKNOWLEDGEMENTS

We thank Anthony Thomas Milliken, ELS, at Editing Synthese (<https://editingsynthese.com>) for his help with editing this manuscript.

COMPLIANCE WITH ETHICAL STANDARDS

All authors were well informed of the WMA Declaration of Helsinki (Ethical Principles for Medical Research Involving Human Subjects) and confirmed that the present study firmly fulfilled the declaration.

INFORMED CONSENT

Not applicable.

CONFLICT OF INTEREST

The authors declare that they have no conflict of interest.

FUNDING SOURCES

None.

ORCID

S.B. Cho  <http://orcid.org/0000-0001-6748-5071>

REFERENCES

1. Taheri A, Mansoori P, Sandoval LF, Feldman SR, Pearce D, Williford PM. Electrosurgery: part I. Basics and principles. *J Am Acad Dermatol* 2014; 70: 591.e1-591.e14.
2. Cosman ER Jr., Cosman ER Sr. Electric and thermal field effects in tissue around radiofrequency electrodes. *Pain Med*. 2005;6: 405-424.
3. Sadick NS, Makino Y. Selective electro-thermolysis in aesthetic medicine: a review. *Lasers Surg Med*. 2004;34:91-97.

4. Taheri A, Mansoori P, Sandoval LF, Feldman SR, Williford PM, Pearce D. Entrance and propagation pattern of high-frequency electrical currents in biological tissues as applied to fractional skin rejuvenation using penetrating electrodes. *Skin Res Technol*. 2014;20:270-273.
5. Zheng Z, Goo B, Kim DY, Kang JS, Cho SB. Histometric analysis of skin-radiofrequency interaction using a fractionated microneedle delivery system. *Dermatol Surg*. 2014;40:134-141.
6. Na J, Zheng Z, Dannaker C, Lee SE, Kang JS, Cho SB. Electromagnetic initiation and propagation of bipolar radiofrequency tissue reactions via invasive non-insulated microneedle electrodes. *Sci Rep*. 2015;5:16735.
7. Chu KF, Dupuy DE. Thermal ablation of tumours: biological mechanisms and advances in therapy. *Nat Rev Cancer*. 2014;14:199-208.
8. Golberg A, Bruinsma BG, Uygun BE, Yarmush ML. Tissue heterogeneity in structure and conductivity contribute to cell survival during irreversible electroporation ablation by "electric field sinks". *Sci Rep*. 2015;5:8485.
9. Yarmush ML, Golberg A, Serša G, Kotnik T, Miklavčič D. Electroporation-based technologies for medicine: principles, applications, and challenges. *Annu Rev Biomed Eng*. 2014;16:295-320.
10. Golberg A, Yarmush ML. Nonthermal irreversible electroporation: fundamentals, applications, and challenges. *IEEE Trans Biomed Eng*. 2013;60:707-714.
11. Dromi SA, Walsh MP, Herby S, et al. Radiofrequency ablation induces antigen-presenting cell infiltration and amplification of weak tumor-induced immunity. *Radiology*. 2009;251:58-66.
12. Rughetti A, Rahimi H, Rossi P, et al. Modulation of blood circulating immune cells by radiofrequency tumor ablation. *J Exp Clin Cancer Res*. 2003;22:247-250.
13. Sluijter ME, Cosman ER, Rittman WB, Van Kleef M. The effects of pulsed radiofrequency fields applied to the dorsal root ganglion: a preliminary report. *Pain Clin*. 1998;11:109-117.
14. Salter DC. Examination of stratum corneum hydration state by electrical methods. *Curr Probl Dermatol*. 1998;26:38-47.
15. Zhao M, Song B, Pu J, et al. Electrical signals control wound healing through phosphatidylinositol-3-OH kinase-gamma and PTEN. *Nature*. 2006;442:457-460.
16. Keese CR, Wegener J, Walker SR, Giaever I. Electrical wound-healing assay for cells in vitro. *Proc Natl Acad Sci USA*. 2004;101:1554-1559.
17. Golberg A, Khan S, Belov V, et al. Skin rejuvenation with non-invasive pulsed electric fields. *Sci Rep*. 2015;5:10187.

How to cite this article: Cho SB, Na J, Zheng Z, et al. In vivo skin reactions from pulsed-type, bipolar, alternating current radiofrequency treatment using invasive noninsulated electrodes. *Skin Res Technol*. 2018;00:1-8.
<https://doi.org/10.1111/srt.12433>